Framework Composition Effects on the Performance of Steam-Activated FeMFI Zeolites in the N_2O-Mediated Propane Oxidative Dehydrogenation to Propylene

Javier Pérez-Ramírez* and Amalia Gallardo-Llamas

Laboratory for Heterogeneous Catalysis, Catalan Institution for Research and Advanced Studies (ICREA) and Institute of Chemical Research of Catalonia (ICIQ), Av. Països Catalans 16, E-43007, Tarragona, Spain

Received: August 9, 2005

The N_2O-mediated oxidative dehydrogenation of propane (ODHP) to propylene has been investigated in the temperature range of 673−773 K over steam-activated FeMFI zeolites with different framework compositions (Si−Al, Si−Ga, Si−Ge, and pure Si). The catalysts, which were characterized by ICP-OES, XRD, SEM, N_2 adsorption, NH_3-TPD, and FTIR of pyridine adsorbed, HRTEM, and UV/vis, have a very similar iron content (0.6−0.7 wt %). A tapered element oscillating microbalance (TEOM) coupled to on-line analysis of products has been applied to simultaneously monitor activity and mass changes during the ODHP reaction. FeAlMFI and FeGaMFI zeolites display higher propylene yields (up to 25%) and a much slower deactivation due to coking than do FeGeMFI and FeMFI zeolites. The higher density and strength of acid sites in the former samples did not induce a faster catalyst deactivation. In general, catalyst deactivation was accelerated upon decreasing the reaction temperature. The total amount of coke formed in the samples during 400 min on stream ranged from 6 to 23 wt %, increasing linearly with the amount of propylene produced. The distinct performance of both groups of zeolites is likely related to the different iron speciation, which is influenced by the composition of the framework. The smaller primary crystallites of FeAlMFI and FeGaMFI, as well as the presence of mesopores in these samples, which are created by dislodgement of aluminum and gallium to extraframework positions, appear to be also beneficial for higher catalyst effectiveness and a reduced deactivation.

1. Introduction

The unique catalytic properties of iron introduced in pentasyl type zeolite matrixes for N_2O-mediated oxidations were originally evidenced by the accomplishments in direct hydroxylation of paraffins to alcohols and of aromatic hydrocarbons to phenols.[1,2] The one-step hydroxylation of benzene with N_2O over iron-containing ZSM-5 leads to phenol selectivities >95% and productivities of 0.4 kg of phenol per hour and kg of catalyst, and has been recently developed on a commercial scale by Solutia and the Boreskov Institute of Catalysis (AlphOx process).[3,4] A direct catalytic route to phenol presents obvious advantages as compared to the conventional three-step cumene peroxidation process, avoiding cumene as intermediate as well as large amounts of acetone as byproduct.

Emerging applications of iron-containing zeolites in oxidative transformations involve the functionalization of light alkanes for obtaining petrochemicals directly or their respective olefinic feedstocks, focusing on the oxidative dehydrogenation of propane (ODHP) to propylene with N_2O over Fe-ZSM-5.[5−8] As was concluded recently, the preparation method of Fe-ZSM-5, that is, how iron is incorporated in the aluminosilicate matrix, is essential to obtain a highly active and selective catalyst. Propylene yields in the range of 22−25% have been obtained over steam-activated Fe-ZSM-5 at 723−773 K,[6,9] which are comparable to the highest values reported over state-of-the-art V- and Mo-based catalysts with O_2 as the oxidant.[10] Steam treatment of the isomorphously substituted iron zeolite is required for achieving superior performances, because framework iron is virtually inactive in the reaction.[11] Postsynthesis incorporation of iron in commercially available zeolites, by liquid-ion exchanged or chemical vapor deposition, led to markedly lower propylene yields (9−16%).[9]

A drawback of iron-containing zeolites in ODHP with N_2O is the deactivation by coke, which causes a rapid decrease of the propylene yield. Previous studies have evidenced the suitability of the TEOM (tapered element oscillating microbalance) technique to investigate deactivation and regeneration of steam-activated Fe-ZSM-5 in ODHP by simultaneous measurement of reaction and mass changes.[11,12] With this information, a cyclic process for continuous propylene production with alternation of reaction, purging, and regeneration steps was engineered using a battery of parallel fixed-bed reactors.[12,13]

The influence of the framework composition of the MFI zeolite on the ODHP reaction over steam-treated Fe-MFI catalysts has not been investigated so far and is required for further optimization of their promising catalytic properties. Pirutko et al.[14] studied the oxidation of benzene to phenol (BTOP) with N_2O over MFI matrixes of various compositions (pure Si, B−Si, Ti−Si, Ga−Si, and Al−Si) with different iron contents and activated in 50 vol % H_2O in He at 923 K. These authors concluded that the purely siliceous as well as the B- and Ti-containing catalysts required 10−100 times more iron to display the same activity as the Al- and Ga-containing catalysts. Based on this, it was suggested that the formation of α-sites (iron species responsible for BTOP) is more favorable over zeolites with Brønsted acidity than over neutral zeolites. However, a direct influence of Brønsted and Lewis acid centers on the reaction mechanism was excluded. Other authors also

* Corresponding author. Fax: +34 977 920 224. E-mail: jperez@iciq.es.

10.1021/jp054447b CCC: $30.25
Published on Web 10/12/2005

concluded that the surface acidity was not responsible for the activity of iron-containing zeolites in the hydroxylation of benzene to phenol with N_2O.[15−18] Studies by the group of Forni have shown that the acidity of iron-containing MFI zeolites (FeAlZSM-5 and Fe-silicalite) is involved in catalyst deactivation by coke formation, which is favored by the strong adsorption of phenol on Lewis acid sites.[15,16] Unfortunately, Pirutko et al.[14] did not investigate the effect of the framework composition on the catalyst deactivation in BTOP, because activity data corresponding to a reaction time of 30 min were only reported.

The present work was undertaken to systematically investigate the influence of the composition of the matrix on the initial performance and deactivation behavior of steam-activated FeMFI zeolites in ODHP with N_2O for propylene production. To this end, zeolites with four different frameworks (Al−Si, Ga−Si, Ge−Si, and pure Si) and very similar iron content (0.6−0.7 wt %) were synthesized and steam-activated under identical conditions, and characterized by ICP-OES, XRD, SEM, N_2 adsorption, NH_3-TPD, FTIR of pyridine adsorbed, HRTEM, and UV/vis. The performance of the resulting materials was assessed in a tapered element oscillating microbalance (TEOM) coupled to on-line gas chromatographic analysis of products in the temperature range of 673−773 K.

2. Experimental Section

2.1. Catalysts. Details on the hydrothermal synthesis of the MFI zeolites with Fe−Al−Si, Fe−Ga−Si, Fe−Ge−Si, and Fe−Si frameworks, as well as the calcinations and ion-exchange treatments previous to steam activation, have been described elsewhere.[19,20] The nominal molar ratios in the synthesis gels were TPAOH/Si = 0.1, NaOH/Si = 0.2, H_2O/Si = 45, Si/(Al or Ga) = 35, Si/Ge = 250, and Si/Fe = 150. The calcined zeolites were activated in steam (300 mbar H_2O in 30 mL of STP N_2 min^{-1} for 5 h) at 873 K. Throughout the manuscript, the catalysts are denoted making reference to the framework composition, that is, FeAlMFI, FeGaMFI, FeGeMFI, and FeMFI. The prefix "c-" refers to the calcined zeolites, while the bare zeolite name relates to the steamed zeolites.

2.2. Characterization. Chemical composition of the samples was determined by ICP-OES (Perkin-Elmer Plasma 40 (Si) and Optima 3000DV (axial)). Powder X-ray diffraction patterns were measured in a Philips X'Pert diffractometer with Bragg−Brentano geometry, and Cu Kα radiation ($\lambda = 0.1541$ nm). Data were collected in the 2θ range of 5−55° using a step size of 0.02° and a counting time of 5 s. Scanning electron microscopy images were recorded at 5 kV in a JEOL JSM-6700F field-emission microscope. Samples were coated with palladium to create contrast. N_2 adsorption at 77 K was carried out in a QuantaChrome Autosorb-6B apparatus. Samples were previously evacuated at 623 K for 16 h. The micropore volume (V_{micro}) and the macropore and mesopore surface area (S_t) were determined with the *t*-plot method according to Lippens and de Boer.[21] The BET method[22] was used to calculate the total surface area (S_{BET}) of the samples, which is used for comparative purposes. Temperature-programmed desorption of ammonia was conducted in a Micromeritics TPR/TPD 2900 equipped with a thermal conductivity detector (TCD). The sample (35 mg) was pretreated at 823 K in He (30 mL min^{-1}) for 1 h. Afterward, pure NH_3 (40 mL min^{-1}) was adsorbed at 473 K for 15 min. Subsequently, a flow of He (30 mL min^{-1}) was passed through the reactor during 30 min to remove weakly adsorbed ammonia on the zeolite. This procedure was repeated three times. Desorption of NH_3 was monitored in the range of 473−823 K at 10 K min^{-1}. The surface acidity of selected zeolite samples was studied by FTIR spectroscopy of adsorbed pyridine. Spectra were recorded using a Bruker IFS 66 spectrometer equipped with a heatable and evacuable reaction cell with CaF_2 windows, which is connected to gas-dosing and evacuation systems. The zeolite powder was pressed into self-supporting wafers with a diameter of 20 mm and a weight of 50 mg. Prior to pyridine adsorption, the samples were pretreated in flowing air at 673 K for 1 h followed by cooling to 373 K. Pyridine was then adsorbed at 373 K for 1 h with bubbling of the Ar flow through a pyridine-containing saturator. Physically adsorbed pyridine was partially evacuated during 5 min at 373 K, and infrared spectra were recorded at different temperatures in the range of 373−673 K with 2 cm^{-1} resolution and 100 scans. High-resolution transmission electron microscopy (HRTEM) was carried out on a Philips CM 30 T electron microscope with a LaB_6 filament as the source of electrons operated at 300 kV. The zeolites were amorphized by the electron beam to enhance the visibility of the small iron oxide particles. Ex situ UV/vis-DRS (diffuse reflectance spectroscopy) measurements of the steamed iron zeolites were performed with a Cary 400 spectrometer (Varian) equipped with a diffuse reflectance accessory (Praying Mantis, Harrick). To reduce light absorption, samples were diluted with α-Al_2O_3 (calcined at 1473 K for 4 h) in a ratio of 1:3. The measured spectra were converted into Kubelka−Munk functions.

2.3. TEOM Studies. Reaction and coke deactivation studies were carried out in a Rupprecht and Patashnick TEOM 1500 pulse mass analyzer coupled to on-line gas chromatography. The TEOM microreactor (4 mm i.d.) was loaded with 30 mg of catalyst (sieve fraction 125−200 μm), firmly packed between two plugs of quartz wool. Prior to experiments, the catalysts were pretreated in flowing He at the reaction temperature for 2 h. When a stable baseline was reached, He was replaced by the reaction mixture, and mass changes and product gases were continuously monitored. The oxidative dehydrogenation of propane with N_2O was carried out in the temperature range of 673−773 K in a mixture of 100 mbar C_3H_8 and 100 mbar N_2O in He at a total pressure of 2 bar and a weight-hourly space velocity (WHSV) of 400 000 mL h^{-1} g_{cat}^{-1}. A fresh sample was used in each run. The coke content was determined from the total mass uptake measured by the TEOM during reaction, accounting for the mass change caused by the change of gas density in the tapered element when He was replaced by the reaction mixture.[13] The product gases were analyzed by an on-line micro-GC (Chrompack CP-2002) equipped with a TCD, using Poraplot Q and Molsieve 5A columns. The conversions of N_2O and C_3H_8 were determined from the amounts of N_2 formed and C_3H_8 disappeared, respectively. Propylene yield and selectivity were calculated as $Y(C_3H_6) = C(C_3H_6)/C°(C_3H_8)$ and $S(C_3H_6) = Y(C_3H_6)/X(C_3H_8)$, respectively, where $C(C_3H_6)$ is the outlet propylene concentration at a certain time, $C°(C_3H_8)$ is the inlet concentration of propane, and $X(C_3H_8)$ is the conversion of propane.

3. Results

3.1. Catalyst Characterization. *Chemical Composition, XRD, and SEM.* Table 1 shows the chemical composition of the steamed FeMFI zeolites. The values obtained in the solids were close to the nominal values in the synthesis gels. The iron content in the samples is very similar (0.6−0.7 wt % Fe), making the comparison of their characterization and catalytic performance data straightforward. The concentration of sodium in the catalysts was below the detection limit of the technique (<0.01 wt %).

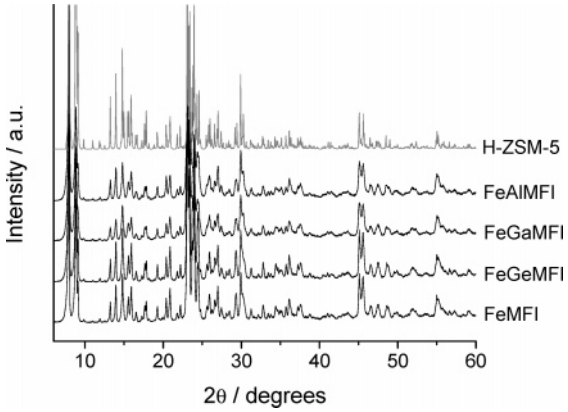

Figure 1. XRD patterns of the steam-activated iron zeolites, including a reference H-ZSM-5.[23]

TABLE 1: Chemical Composition of the Zeolite Samples

sample	Si (wt %)	Fe (wt %)	Ge (wt %)	Ga (wt %)	Al (wt %)
FeMFI	44.65	0.68			
FeGeMFI	43.40	0.67	0.44		
FeGaMFI	42.44	0.59		3.23	
FeAlMFI	40.98	0.67			1.26

No evidence of any other phase besides ZSM-5 was found in the XRD patterns of the steamed zeolites in Figure 1. The relative intensity and width of the reflections are similar in the four samples, suggesting a similar degree of crystallinity. Further assessment of the size, distribution, and morphology of the zeolite crystals was derived from SEM analysis (Figure 2). The typical intergrowth phenomenon can be clearly distinguished in the samples. Besides, the crystallite size distribution is rather uniform and no amorphous matter was detected at the external surface. Low-magnification images show that FeGeMFI and FeMFI consist of zeolite particles of ca. 1 μm, being larger in FeAlMFI and FeGaMFI (ca. 2 μm). However, the morphology of the zeolite particles in these two groups of samples is remarkably different. As exemplified by the high-resolution micrograph of FeAlMFI in Figure 2, the particles in the Al and Ga-containing zeolites are constituted by agglomerates of very small crystallites, which are orderly packed parallel to each other. Contrarily, FeMFI and FeGeMFI result in larger primary crystallites with a smooth surface.

N_2 Adsorption. Nitrogen adsorption was performed to investigate the porous properties of the zeolites. As shown in Table 2, the total pore volumes of the steam-activated samples are similar. The N_2 isotherms of FeMFI and FeGeMFI in Figure 3 exhibit high nitrogen uptakes at low relative pressures ($p/p_o < 0.3$) and a plateau at high relative pressures, being typical for microporous materials (type I according to IUPAC classification[24]). Application of the BET model and the *t*-plot method confirms that the majority of the surface area ($S_{BET} = 433$ and 426 $m^2\ g^{-1}$ for FeMFI and FeGeMFI, respectively) is due to the presence of micropores, while the contribution of mesoporosity and macroporosity is relatively small ($S_t = 10-13\ m^2\ g^{-1}$).

TABLE 2: Textural Properties of the Iron-Containing Zeolites

sample	V_{total} ($cm^3\ g^{-1}$)	V_{micro}[a] ($cm^3\ g^{-1}$)	S_t[a] ($m^2\ g^{-1}$)	S_{BET}[b] ($m^2\ g^{-1}$)
FeMFI	0.23	0.19	13	433
FeGeMFI	0.22	0.19	10	426
FeGaMFI	0.24	0.15	51	388
FeAlMFI	0.23	0.16	33	380
c-FeAlMFI	0.21	0.17	23	410

[a] *t*-plot method.[21] [b] BET method.[22]

The isotherms of the steamed FeGaMFI and FeAlMFI present a behavior similar to that of the other two zeolites at low relative pressures, but additionally exhibit hysteresis in the adsorption−desorption isotherm at $p/p_o > 0.45$. This can be attributed to the formation of certain mesoporosity as a consequence of the partial extraction of aluminum and gallium upon steam treatment to nonframework positions, as has been demonstrated elsewhere by ^{71}Ga and ^{37}Al MAS NMR.[20,25] The hysteresis is absent previous to the steam treatment, as evidenced in the isotherm of the calcined c-FeAlMFI sample (open symbols in Figure 3). The latter isotherm is nearly identical to those of calcined FeGeMFI and FeMFI, which are not shown because they did not change upon steam treatment. The creation of mesoporosity in the steamed FeAlMFI and FeGaMFI zeolites is also supported by the slightly decreased micropore volume (Table 2) and the decreased uptake at low pressure as compared to the calcined samples (compare isotherms of calcined and steamed FeAlMFI in Figure 3). Associated with this, an increase of the mesopore area and a decrease of the BET surface area in FeGaMFI and FeAlMFI with respect to FeGeMFI and FeMFI were obtained. Although the validity of the BET model for highly microporous materials is questionable, the surface areas derived from this model in the adapted pressure range $p/p_0 = 0.01-0.10$ can be used for comparative purposes.[26]

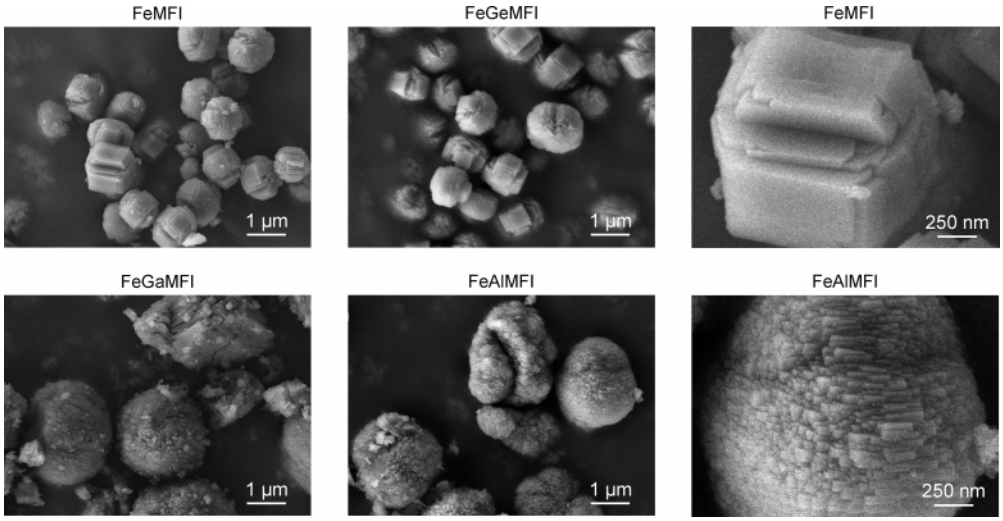

Figure 2. SEM micrographs of the steam-activated iron zeolites.

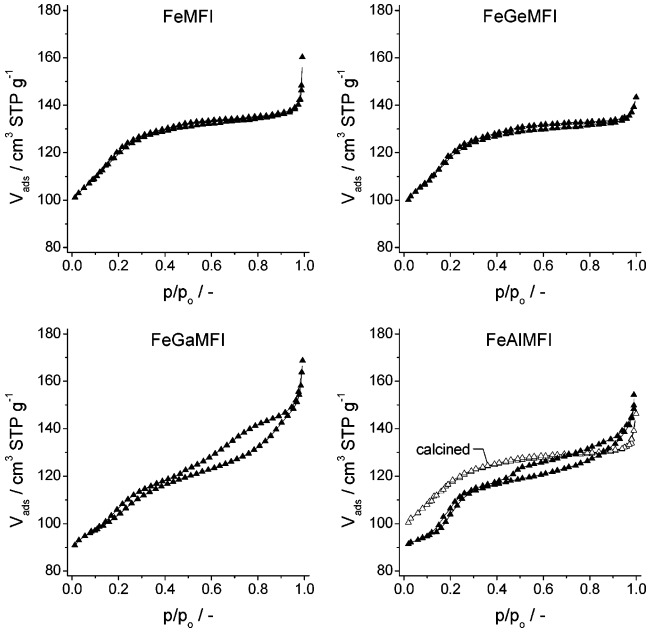

Figure 3. N_2 adsorption−desorption isotherms at 77 K of the steam-activated iron zeolites. The isotherm of calcined FeAlMFI (open symbols) is shown for comparative purposes.

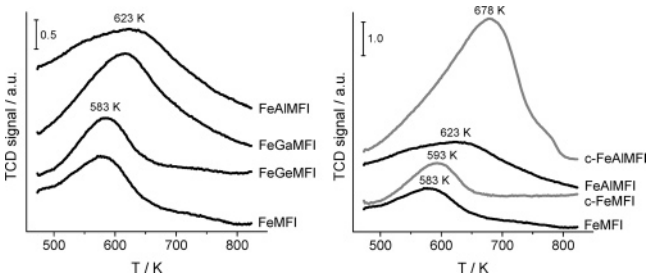

Figure 4. NH_3-TPD profiles of the iron-containing zeolites.

Acidity. Temperature-programmed desorption of ammonia was used to investigate the acidic properties of the calcined and steamed iron zeolites. This method cannot be applied for a definitive assignment of the desorbed ammonia to Brønsted and Lewis acid sites.[27] Nevertheless, it provides a valuable fingerprint of the relative strength and distribution of the acidity, and a quantification of the density of total acid sites. Attending to the position of maximum in the NH_3-TPD profiles (Figure 4), the stronger acidity of steam-treated FeAlMFI and FeGaMFI (peak at 623 K) as compared to FeGeMFI and FeMFI (peak at 583 K) can be safely concluded. Based on the position of the peak maxima, the similar nature of acid centers in these two groups of zeolites (Si−Al and Si−Ga vs Si−Ge and pure Si) can be inferred. The ammonia uptake in Figure 5 shows that the density of acid sites in steamed FeAlMFI and FeGaMFI zeolites (0.15−0.17 mmol NH_3 g^{-1}) is 2−3 times higher than that in FeGeMFI and FeMFI (0.05−0.08 NH_3 g^{-1}). However, the strength and density of acidic centers in the steamed Al- and Ga-containing samples are relative weak and small as compared to the respective calcined precursors (cf. Figures 4 and 5). For example, the calcined FeAlMFI exhibits an ammonia uptake of 0.46 mmol NH_3 g^{-1}, and the maximum in the desorption profile was situated at 678 K. This feature is typically assigned to Brønsted acids arising from the presence of Al in framework positions. As commonly described,[18,20,25] the decreased density and strength of the acidic centers in steamed zeolites is caused by the massive dislodgement of a trivalent cation isomorphously substituted (M = Al, Ga, Fe, etc.) due to the hydrolysis of Si−O(H)−M bonds. This fact induced the formation of mesopores in the corresponding zeolites. As expected, only minor changes in ammonia uptake and adsorption isotherms were observed upon steam treatment of FeGeMFI and FeMFI zeolites as compared to FeAlMFI and FeGaMFI, confirming that Al and Ga were mainly responsible for the decreased acidity and formed porosity. This can be expected in view of the 4 times higher content of aluminum and gallium in the samples as compared to iron (cf., Table 1).

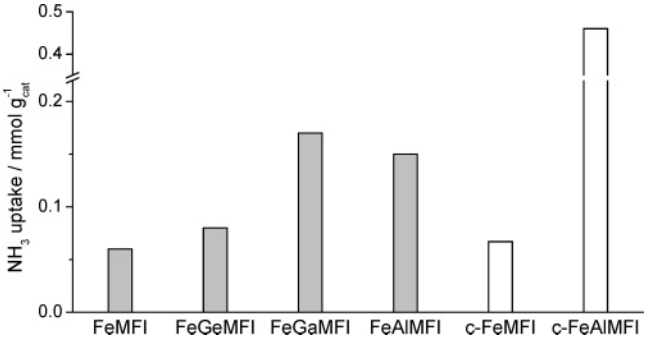

Figure 5. Ammonia uptake of the iron-containing zeolites in NH_3-TPD experiments.

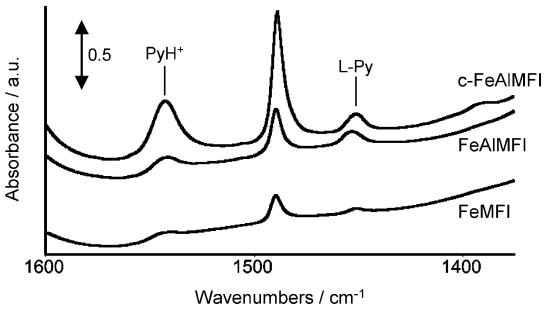

Figure 6. FTIR spectra of pyridine adsorbed on selected iron zeolites at 523 K. Background spectra of the air-pretreated samples were subtracted.

TABLE 3: Areas (in arbitrary units) of the Absorption Bands in the FTIR Spectra of Selected Zeolites at 523 K of Pyridine Adsorbed Associated with Brønsted (PyH^+) and Lewis (L-Py) Acidity and the Corresponding Ratio

sample	PyH^+, 1545 cm^{-1}	L-Py, 1445 cm^{-1}	PyH^+/L-Py
FeMFI	0.5	0.2	2.5
FeAlMFI	1.0	1.1	0.9
c-FeAlMFI	5.3	1.2	4.4

FTIR spectroscopy of pyridine adsorbed was conducted over selected samples to complement the NH_3-TPD results. This technique makes it possible to discriminate between Brønsted and Lewis acidity. Details of the assignment of the bands of pyridine adsorbed described below are elaborated in the literature.[28−30] Figure 6 shows the infrared spectra of pyridine adsorbed at 523 K over the calcined and steamed FeAlMFI zeolites and the steamed FeMFI zeolite. The bands at 1545 and 1450 cm^{-1} are characteristic of pyridine adsorbed on Brønsted acid sites (PyH^+) and Lewis acid sites (L-Py), respectively. The ratio of Brønsted to Lewis acidity in Table 3 was determined from the areas of these bands, because the ratio of the extinction coefficients of these two absorptions is ∼1.[31−33] The spectrum of 523 K was selected for quantification to exclude any contribution of hydrogen-bonded pyridine (hb-Py) at 1445 cm^{-1}. These two forms of pyridine adsorbed overlap at 1545 cm^{-1}, and spectral quantification at T < 523 K would thus overestimate the Lewis acidity.[34] The temperature dependences of the

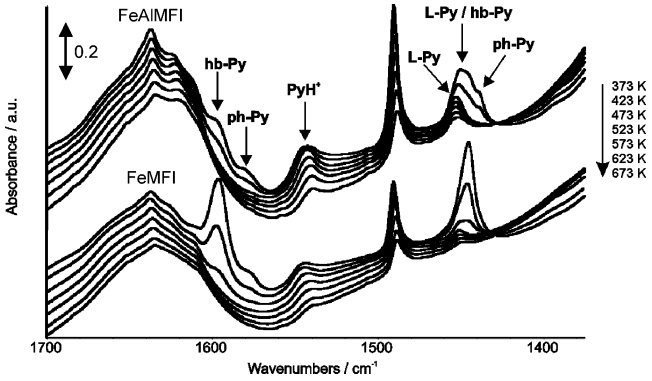

Figure 7. FTIR spectra of pyridine adsorbed on FeMFI and FeAlMFI at different temperatures. Subtraction of background spectra was not applied.

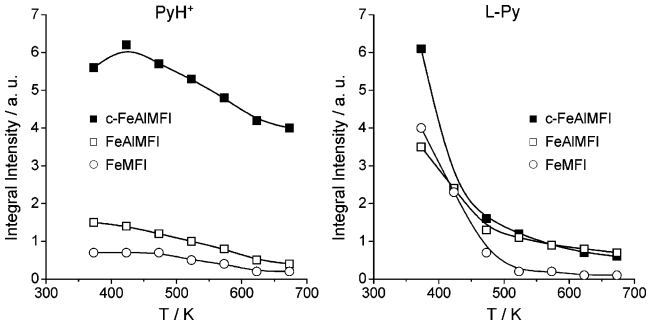

Figure 8. Change of the FTIR band area for pyridium ions (PyH^+) at 1545 cm^{-1} and for pyridine coordinated to Lewis acid sites (L-Py) at 1445 cm^{-1} versus desorption temperature over selected iron zeolites.

infrared spectra over the steamed samples in Figure 7 clearly demonstrate the complete desorption of hb-Py from 523 K upward, as concluded from the disappearance of the band at 1590 cm^{-1}. It is also observed that the bands at 1440 and 1580 cm^{-1}, which are related to physically adsorbed pyridine (ph-Py), vanished already at 473 K.

The results from the spectral quantification in Table 3 conclude that steam treatment of FeAlMFI reduces the amount of Brønsted acid sites by a factor of 5, while the amount of Lewis acid sites is only slightly decreased. The total density of acid sites (the sum of total Brønsted and Lewis acid sites) was decreased by 68% from upon steam-treatment of calcined FeAlMFI, in excellent agreement with the 70% value determined from the ammonia uptake in NH_3-TPD experiments (Figure 5). The amount of Brønsted and Lewis acidic centers in steamed FeAlMFI is ca. 2 and 5 times higher as compared to steamed FeMFI, respectively. Globally, the total density of acid sites from pyridine adsorption was 67% lower in steam-treated FeMFI as compared to steam-treated FeAlMFI, which is in excellent agreement with the value determined from the ammonia uptake in NH_3-TPD.

Figure 8 displays the dependence of the area of the bands at 1545 cm^{-1} (PyH^+) and 1445 cm^{-1} (L-Py) with temperature. For all of the samples, the band at 1445 cm^{-1} sharply decreases upon increasing the temperature in the range 373−500 K due to the significant contribution of hb-Py in the Lewis acidity region at these low temperatures (vide supra). The similar slope of the intensity versus temperature dependences above 523 K, at which hb-Py is completely desorbed, is indicative of a comparable stability of pyridine on strong Lewis acid and Brønsted acid sites and suggests a similar acidic strength. This agrees with the findings of Meloni et al.,[15] who detected an even higher stability of pyridine adsorbed on Lewis than on

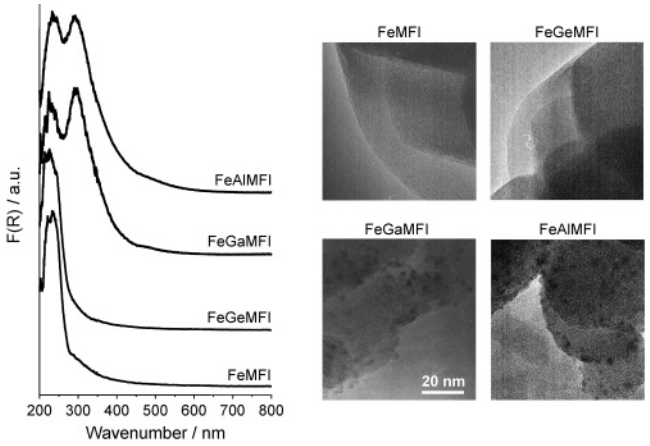

Figure 9. UV/vis spectra and HRTEM micrographs of the steam-activated iron zeolites (adapted from ref 19).

Brønsted acid sites in steam-treated Fe-silicalite, as compared to steam-treated Fe−ZSM-5.

Forms of Iron. HRTEM and UV/vis techniques were applied to compare the type of iron species in the steam-treated zeolites. The visual appearance of the samples already suggests different iron constitutions. FeAlMFI and FeGaMFI are light brownish, which indicates a certain accumulation of iron oxide/hydroxide in the zeolite. FeGeMFI and FeMFI were a very pale tonality, nearly white, suggesting the more isolated nature of the iron species in these catalysts. The HRTEM micrographs of the Al- and Ga-containing samples in Figure 9 confirmed the presence of iron oxide nanoparticles with a homogeneous size distribution (1−2 nm), which were certainly not visible in FeGeMFI and FeMFI. As mentioned above and elaborated elsewhere,[20,25] steam treatment of FeAlMFI and FeGaMFI not only leads to a complete dislodgment of framework iron, but also induces an extensive extraction of aluminum and gallium species to extralattice positions. Accordingly, the presence of Al (or Ga) in the iron oxide nanoparticles cannot be excluded.

The UV/vis spectra of the samples are in good agreement with HRTEM studies. FeAlMFI and FeGaMFI in Figure 9 show two intense $Fe^{3+}\leftarrow O$ charge-transfer (CT) bands at 250 and 300 nm, as well as a smaller contribution at 500 nm. A detailed assignment of these bands is given elsewhere.[35−38] Briefly, bands between 200 and 300 nm are typically attributed to isolated Fe^{3+} species, either tetrahedrally coordinated in the zeolite framework or with higher coordination. Octahedral Fe^{3+} ions in small oligonuclear $Fe^{3+}_xO_y$ complexes give rise to broad bands between 300 and 450 nm, and bands above 450 nm are characteristic of Fe^{3+} ions in large iron oxide aggregates. These are clearly associated with the nanoparticles identified by HRTEM. Contrarily, the UV/vis spectra of FeMFI and FeGeMFI display a single CT band at 236 nm, indicating that the majority of Fe^{3+} species in the samples is well isolated. The contribution at 300 nm indicates a minor degree of iron association in the sample in the form of oligomeric species. No contribution >450 nm is observed, which excludes the presence of iron oxide particles, as concluded from HRTEM. Accordingly, a significant degree of iron association can be concluded in the Al- and Ga-containing zeolites as compared to the Ge-containing and purely siliceous zeolites. Previous investigations concluded that the presence of trivalent cations such as Al^{3+} or Ga^{3+} in the MFI framework facilitates the dislodgement of framework iron atoms and clustering of extracted iron species for a given condition of temperature, water vapor pressure, and duration.[20] This is in line with results from our study, where identical steam-treatment conditions were applied for the four catalysts. In other words,

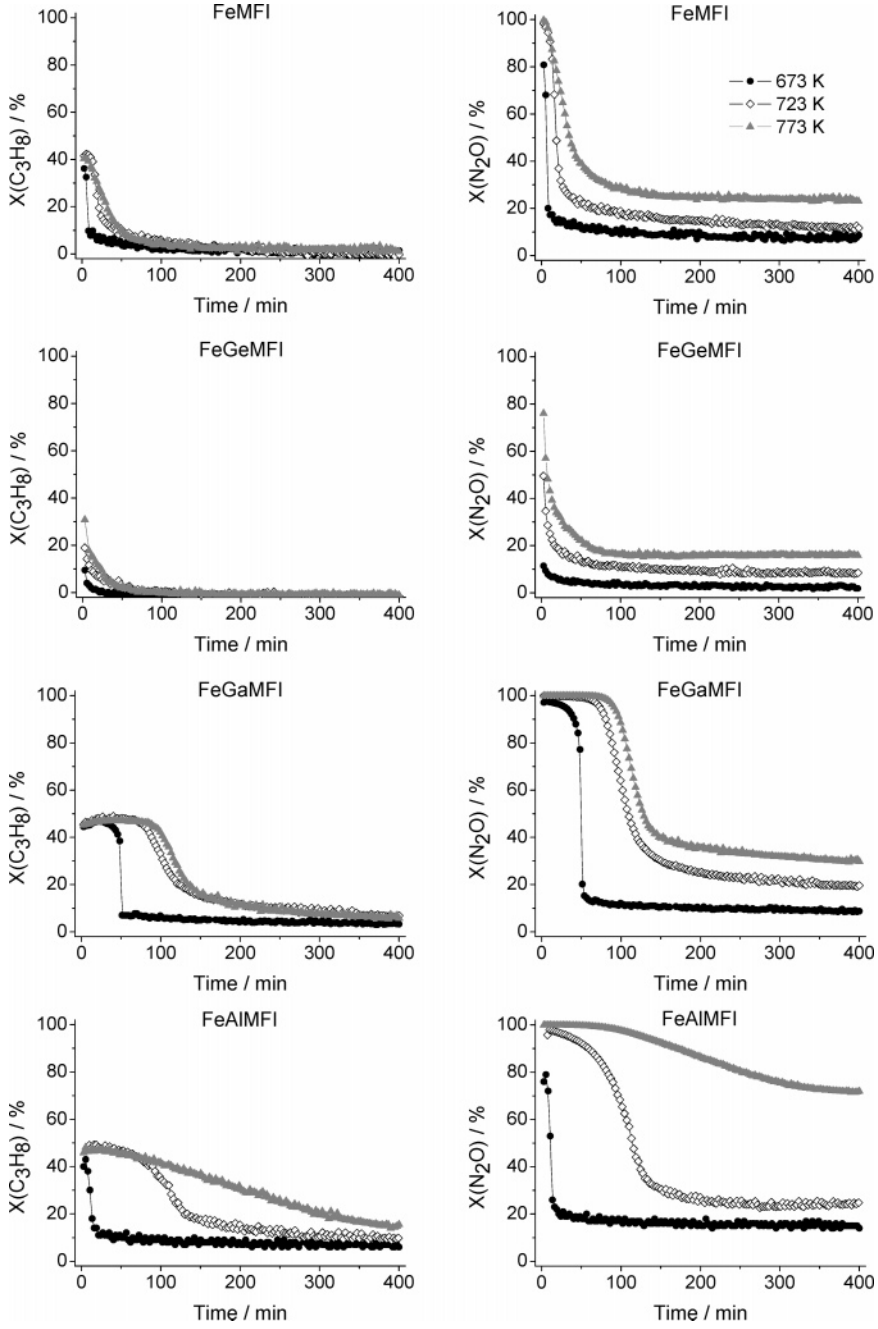

Figure 10. Conversions of N_2O and C_3H_8 during ODHP at different temperatures versus time-on-stream over the steam-activated zeolite catalysts. Conditions: 100 mbar C_3H_8 and 100 mbar N_2O in He, WHSV = 400 000 mL h^{-1} g_{cat}^{-1}, and P = 2 bar.

FeAlMFI and FeGaMFI require milder steaming conditions for achieving the same degree of iron extraction and clustering as compared to FeGeMFI and FeMFI.

Deconvolution of UV/vis bands according to the procedure described in ref 38 has established that the relative percentage of isolated ions, oligonuclear species, and iron oxide particles in FeAlMFI and FeGaMFI was 30%:62%:8% and 25%:64%:11%, respectively, in contrast with the values obtained for FeGeMFI and FeMFI (74%:26%:0% and 70%:30%:0%, respectively). As reasoned elsewhere,[19,38] this quantification did not account for the dependence of the extinction coefficient on the wavelength and the contribution of eventual Fe^{2+} present in the nonpretreated samples, but it certainly provides valuable information about the distinct distribution of the various iron species in the catalysts.

3.2. Catalytic Performance in ODHP. *Initial Activity.* Figures 10 and 11 show the catalytic performance of the steam-activated iron zeolites versus time-on-stream during ODHP with N_2O in the temperature range of 673−773 K, as derived from the TEOM experiments and coupled gas chromatographic analysis. Reaction data after 2 min on stream (called initial performance, t_o) and after 400 min on stream (called final or residual performance, t_f) are summarized in Table 4. The initial conversion of the reactants and propylene yield are a function of the temperature and catalyst sample in question. The initial N_2O conversion significantly increases with temperature, particularly when going from 673 to 723 K. FeGaMFI, FeAlMFI, and FeMFI exhibit complete N_2O conversions at 723 and 773 K. The conversion over FeGeMFI was remarkably lower (only 11% at 673 K and up to 76% at 773 K). The C_3H_8 conversion typically varied in the range of 36−48%, increasing moderately with temperature over FeMFI and FeAlMFI and being practically independent of temperature over FeGaMFI. FeGeMFI also presents a relatively low initial propane conversion at 673 K

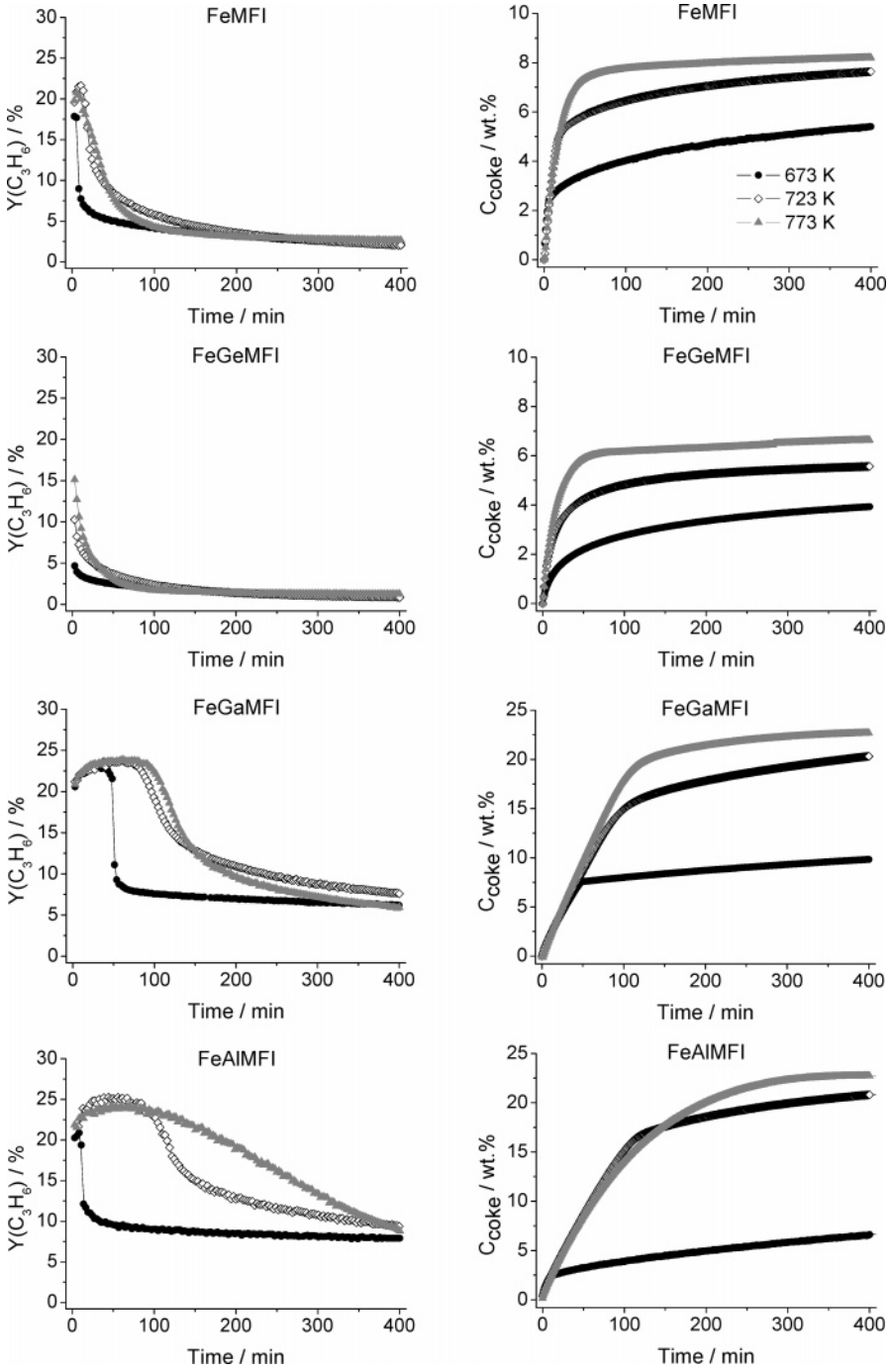

Figure 11. Yield of C_3H_6 and coke content during ODHP at different temperatures versus time-on-stream over the steam-activated zeolite catalysts. Conditions are as in the caption of Figure 10.

(10%), increasing to 31% at 773 K. Despite the different degrees of propane conversion, the initial propylene selectivity varied in a narrow range of 46−54% in all of the tests with the different catalysts. FeAlMFI and FeGaMFI displayed the highest initial propylene yield (20−22%), followed by FeMFI (18−20%), and finally FeGeMFI, for which the C_3H_6 yield did not exceed the value of 15% at 773 K. It should be stressed that, apart from propylene, other quantified reaction products include carbon oxides, as well as minor amounts of ethane, ethylene, and methane. The concentration of ethylene at the reactor outlet was typically 15−20 times lower than that of propylene. It has been reported that various oxygenates (e.g., propionaldehyde, acrolein, acetone) as well as alcohols and aromatics are also formed in the reaction. These were quantified using conventional gas chromatography with temperature programming that resulted in analysis times in the range of 15−100 min.[6,7] The micro-GC analysis used here certainly does not resolve all components in the product mixture, but is able to separate the reactant (propane) and our target product (propylene) in less than 2 min. As discussed later, the short analysis time proves essential to precisely follow the rapid catalyst deactivation process and to correlate loss in ODHP performance with coke formation.

Time-on-Stream Behavior. The curves in Figures 10 and 11 evidence the different time-on-stream catalytic performance of the various samples. Different deactivation patterns were identified, depending on the zeolite and reaction temperature. For FeMFI and FeGeMFI, an excellent correlation was found between the decrease of the C_3H_6 yield (and C_3H_8 and N_2O conversions) with the increased coke amount in the samples, as expected from catalyst deactivation due to coking.[11,12]

TABLE 4: Catalytic Performance of Steam-Activated Iron Zeolites in ODHP with N_2O

sample	T (K)	$X(N_2O)$ (%)		$X(C_3H_8)$ (%)		$Y(C_3H_6)$ (%)		$S(C_3H_6)$ (%)	C_{coke} (wt %)
		t_o[a]	t_f[b]	t_o	t_f	t_o	t_f	t_o	
FeMFI	673	81	8.5	36	1	18	2	49	5.4
	723	98	12	42	0	20	2	47	7.6
	773	99	23	40	1	20	2	49	8.2
FeGeMFI	673	11	2	10	0	5	1	50	3.9
	723	50	8	19	0	10	1	54	5.6
	773	76	16	31	0	15	1	49	6.6
FeGaMFI	673	97	9	44	3	21	6	46	9.8
	723	100	20	45	7	21	7	47	20.3
	773	100	30	45	6	21	6	46	22.7
FeAlMFI	673	80	14	40	6	20	8	51	6.6
	723	98	25	48	10	22	9	45	20.8
	773	100	72	46	16	22	9	48	22.7

[a] t_o: initial performance (after 2 min on stream). [b] t_f: residual performance (after 400 min on stream).

FeGeMFI exhibits this behavior at all temperatures (cf., Figure 11). The fast decrease of the propylene yield in the first 10−25 min on stream is associated with the steep increase of the coke content in this time period. Afterward, the propylene yield levels off and the coking profile reaches a well-defined plateau. The deactivation pattern of FeMFI resembles that of FeGeMFI, with the exception that the former catalyst displays certain activation in the first 6 min on stream at 723 and 773 K, before the propylene production starts to drop. As exemplified by FeMFI, the decrease of $Y(C_3H_6)$ is less pronounced upon increasing temperature, particularly when going from 673 to 723 K. However, the slope of the initial process of coke build-up is similar, suggesting that the rate of coke formation does not strongly depend on temperature. The amount of coke formed in FeMFI and FeGaMFI ranges from 4 to 8 wt %, increasing with the reaction temperature and being slightly higher over FeMFI (cf., Table 4).

FeGaMFI and FeAlMFI exhibit a similar ODHP behavior, which strongly differs from that of FeMFI and FeGeMFI. First, the former zeolites originate a higher initial propylene yield. Besides that, a marked phenomenon of activation occurs, by which the propylene production increases even if the amount of coke increases. Consequently, the yield of propylene increases from 20 to 22 up to 25% and is stable during a certain period of stable performance of time before deactivation is noticed. This period is typically longer at higher temperatures. For example, at 673 K, FeGaMFI maintains a propylene yield of ca. 22% for ca. 40 min, considerably longer than that in FeAlMFI at the same temperature (ca. 10 min). However, the stability of FeAlMFI is superior to that of FeGaMFI at 773 K. At this temperature, a C_3H_6 yield >20% was maintained over FeAlMFI at 773 K during 175 min. The resistance of FeAlMFI toward deactivation was key to develop a cyclic process for continuous propylene production via alternation of reaction and regeneration steps using a battery of parallel fixed-bed reactors.[13] The final coke content in FeGaMFI and FeAlMFI after the ODHP reaction at 673 K was in the range 7−10 wt %, relatively higher than the values obtained over FeMFI and FeGeMFI at this temperature. The amount of coke formed over the Al- and Ga-containing zeolites increased by a factor of 2−3 upon increasing the reaction temperature, leading to values up to 23 wt % when the reaction was conducted at 773 K (cf., Table 4). The residual activity of FeGaMFI and FeAlMFI is also significantly higher than that of FeMFI and FeGeMFI. Propylene yields in the range of 6−10% were obtained after 400 min on stream over the former group of samples, while the latter group did not exceed propylene yields of 2%. Remarkably, the final propylene yield over each of the catalysts was practically the same at all reaction temperatures.

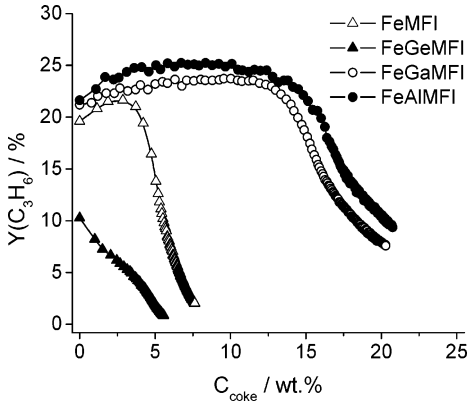

Figure 12. Yield of C_3H_6 versus coke content over the steam-activated iron zeolites at 723 K.

The distinct deactivation behavior of the samples is further highlighted in Figure 12. For FeGeMFI, the propylene yield decreases linearly with the amount of coke in the sample. FeMFI evidences a constant propylene yield up to coke contents of ca. 3 wt % followed by an abrupt (linear) decrease of the olefin production. The characteristics of FeAlMFI and FeGaMFI are very similar: $Y(C_3H_6)$ slightly increases with the coke amount and then remains essentially invariable until the coke content over the zeolite is of ca. 12−13 wt %. The residual activity (after 400 min on stream) increases with the final coke content of the sample in the order FeAlMFI > FeGaMFI > FeMFI > FeGeMFI.

Propylene as the Coke Precursor. The results here and elsewhere[9,11] demonstrate that the decreased propylene yield during ODHP is associated with the build-up of coke deposits in the zeolite samples. In our previous works, propylene condensation was suggested as the main coke precursor. Our present results corroborate this more quantitatively, attending to the correlation between the amount of propylene produced and the amount of coke formed in the 400 min tests at different temperatures (Figure 13). An increased absolute amount of propylene produced, which can also be expressed as a higher average propylene yield, originates an increased amount of coke in the samples following a linear relationship. However, as illustrated in the figure, the increment in coke content (ΔC_{coke}) is approximately double than the increment in the amount of propylene produced ($\Delta n(C_3H_6)$).

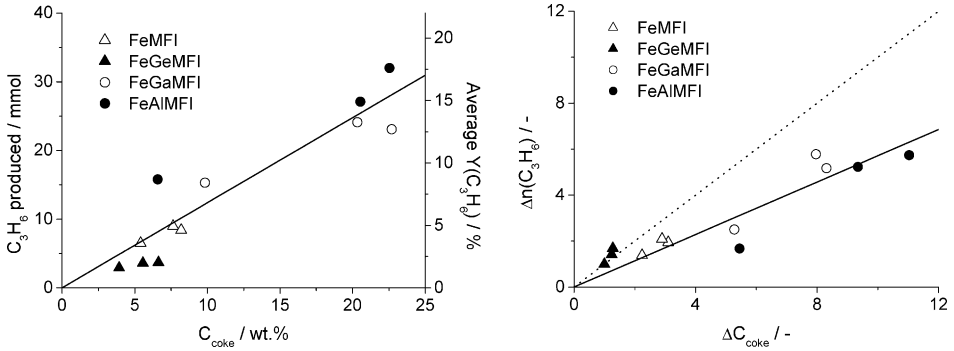

Figure 13. Correlation between the amount of propylene produced and the coke content during the ODHP tests over the steam-activated iron zeolites at the three temperatures investigated.

4. Discussion

The performance of steam-activated iron-containing MFI zeolites in the N_2O-mediated propane oxidative dehydrogenation depends on the composition of the matrix. The Al- and Ga-containing zeolites showed a higher initial activity than the Ge-containing and purely silicious matrixes, and particularly an improved resistance toward deactivation. The higher activity of the more acidic FeAlMFI and FeGaMFI zeolites in ODHP as compared to the more neutral FeGeMFI and FeMFI agrees with the results by Pirutko et al.[14] for the N_2O-mediated benzene-to-phenol (BTOP). As stated in the Introduction, these authors suggested that the presence of Brønsted acidity in the zeolite (induced by Al or Ga) originates more active iron species (α-sites), which are ultimately responsible for the BTOP performance. Pirutko et al.[14] did not evaluate the influence of the matrix composition on the deactivation behavior by coke, which is observed in this reaction.[15,16,39,40] It is here where the zeolite framework has a major effect in the ODHP reaction. This likely applies to the BTOP process too.

The TEOM technique coupled to micro-GC analysis proves as a unique tool to simultaneously determine activity and mass changes due to coking during ODHP. In situ monitoring of coke formation as well short analysis times are key features to derive accurate information on deactivation profiles in fast-deactivating reactions. This level of detail and accuracy cannot be accomplished with typical approaches to study deactivation, where coke is characterized after subjecting the catalyst to activity tests and taking samples for ex situ analyses after a certain period of time. This methodology often results in a limited number of samples, and consequently deactivation patterns cannot be precisely determined. For example, Forni et al.[15,16] investigated the deactivation of steam-treated FeMFI (Fe-ZSM-5 and Fe-silicalite) in BTOP by measuring the activity decay during 6 h on stream (at intervals of 1 h), although the performance at $t \rightarrow 0$ was not determined. The amount and nature of the carbonaceous deposits in the coked samples (after the 6 h run) were determined ex situ. For the same reaction and catalyst type, Ivanov et al.[39,40] obtained more detailed deactivation patterns during 20 h on stream, but only five samples (at 0.5, 1.5, 3, 9, and 20 h) were taken for determination of the coke amount. This contrasts with the 150 activity points during our 400 min runs and the in situ determination of an equivalent number of data points for the coke amount in our TEOM experiments, and highlights the suitability of our methodology for investigating deactivation by coking in N_2O-mediated hydrocarbon conversions over zeolites.

Several features associated with the composition of the original zeolite framework can explain the different catalytic behavior in the ODHP reaction. This includes the morphology and texture of the crystals, as well as the acidity and forms of iron in the steam-treated materials. The characteristics of steam-activated FeAlMFI and FeGaMFI are remarkably similar and so is the catalytic performance. An unexpected result was obtained for FeGeMFI and FeMFI. Despite the very similar characterization results, the Ge-containing sample displayed significantly lower initial C_3H_8 and N_2O conversions and C_3H_6 yield. A negative effect by germanium was not reflected in direct N_2O decomposition, where both FeGeMFI and FeMFI displayed very similar catalytic activities.[19] This observation cannot be conclusively explained at the present stage.

The presence of Al and Ga in the zeolite matrix also provides an easier escape of Fe to extraframework position and promotes iron association at a given steaming condition (temperature and steam partial pressure). In this manner, characterization studies here and elsewhere[19,20,25,34,38] concluded that FeAlMFI and FeGaMFI present a high degree of iron clustering in the form of active iron oxo-clusters and even iron oxide nanoparticles, while the degree of clustering in FeGeMFI and FeMFI is much less extended and a main fraction of iron is stabilized in isolated extraframework positions. It is even so that a certain (minor) fraction of iron in the latter two samples remains in (inactive) framework positions at the steaming conditions applied.[20] Accordingly, it can be suggested that the improved dislodgement of framework iron and the presence of a larger fraction of oligomeric species in the pores of FeAlMFI and FeGaMFI induces the superior ODHP performance with respect to the zeolites without an additional trivalent cation (besides Fe). This includes not only the higher initial propylene yield but mainly the improved resistance toward deactivation by coke. Furthermore, the presence of extraframework iron clusters containing additionally aluminum or gallium may be also beneficial for the catalytic performance. In this respect, Hensen et al.[41,42] have proposed that extraframework Fe−Al−O species, obtained by the high-temperature calcination and steam treatment of Fe-ZSM-5 prepared by chemical vapor deposition, are the active sites in the benzene hydroxylation with N_2O. This reasoning may also apply to explain the lower activity of iron-containing zeolites with pure Si, B−Si, and Ti with respect to Si−Al and Si−Ga matrixes in the BTOP with N_2O.[14]

Additional advantages of having of Al and Ga in the framework of the original zeolite relate to the occurrence of very small crystallites and the presence of mesopores due to expulsion of lattice trivalent atoms during the high-temperature treatment in steam. Both features guarantee a better utilization of the zeolite crystal by enhancing the intrazeolitic transport of reactants and products. Besides, these features induce effects of pore blocking by coke to be retarded, contributing to the improved resistance of these samples toward deactivation as

compared to FeGeMFI and FeMFI. Forni et al.[15,16] stated that deactivation of ZSM-5 in BTOP is caused by blockage of the pores by coke molecules trapped in their intersections. Accordingly, the improved durability of steamed FeZSM-5 with respect to Fe-silicalite was partially attributed to the more open structure of the former zeolite framework caused by the mesoporosity formed. Contrarily, Ivanov et al.[39,40] indicated that deactivation of iron-containing ZSM-5 for the same reaction is caused by coke poisoning of active iron sites, whose concentration decreases linearly with the coke content, rather than by blocking of zeolite pores. Based on this, the authors concluded the absence of diffusion limitations associated with coke formation. The systematic preparation and characterization of iron-containing zeolites and the TEOM investigations strongly suggest that both processes, that is, poisoning of active iron sites and pore blocking, are involved in the mechanism of catalyst deactivation during ODHP. Accordingly, small crystals and the mesopores in the Al- and Ga-containing samples, as well as a more suitable constitution of the iron species, result in more efficient catalytic materials for the reaction.

Finally, Forni et al.[16] also proposed a correlation between the activity loss for phenol production and the concentration of Lewis acid sites in the zeolite, due to the strong interaction of phenoxy groups with this type of acid centers. In the ODHP reaction investigated here, no correlation was found between the density and strength of the acidic centers and the deactivation rate. The Al- and Ga-containing samples have a 2−3 higher density of total acid sites, with ca. 2 and 5 times higher density of Brønsted and Lewis acidity than FeGeMFI and FeMFI, respectively. Despite this, the former samples were considerably less susceptible for deactivation.

5. Conclusions

Our investigations have concluded that the composition of the framework in steam-activated iron-containing MFI zeolites strongly impacts the initial activity and deactivation behavior of the catalysts in the N_2O-mediated oxidative dehydrogenation of propane. In this study, the iron content in the samples and the steam activation conditions were kept identical so as to purely assess framework composition effects. FeAlMFI and FeGaMFI display higher propylene yields and a slower deactivation than FeMFI and FeGeMFI. For identical steam-activation conditions, the presence of aluminum and gallium leads to a higher concentration of iron oxo-clusters stabilized in the zeolite pores. These species appear to be more efficient sites for the ODHP with N_2O than the more isolated nature of the iron species in FeGeMFI and FeMFI zeolites, for which the extraction of (inactive) framework iron is less facilitated. The presence of small amounts of germanium deteriorates the catalytic performance of the iron-containing zeolites in N_2O-mediated ODHP. FeGeMFI is considerably less active than FeMFI even if the forms of iron as well as other (textural and acidic) properties are very similar in both materials. The TEOM technique conclusively shows that deactivation of zeolites in ODHP is due to coke formation. Propylene is the main coke precursor, and a linear relation between the amount of propylene produced by the catalysts and the coke content was obtained. The more acidic FeGaMFI and FeAlMFI matrixes did not lead to an accelerated catalyst deactivation by coking as compared to the more neutral FeGaMFI and FeAlMFI matrixes. On the contrary, the former samples exhibit a marked activation procedure in the first stages of the reaction and a relatively high residual activity. The presence of mesopores in steamed FeAlMFI and FeGaMFI, as well as the small size of the resulting primary crystallites in these samples, can be also responsible for their improved ODHP performance.

Acknowledgment. We are indebted to Dr. U. Bentrup for the FTIR studies presented in this manuscript. J. C. Groen and T. Bach are acknowledged for the N_2 adsorption and SEM analyses, respectively.

References and Notes

(1) Panov, G. I.; Uriarte, A. K.; Rodkin, M. A.; Sobolev, V. I. *Catal. Today* **1998**, *41*, 365.
(2) Panov, G. I. *CATTECH* **2000**, *4*, 18.
(3) Ondrey, G. *Chem. Eng.* **2004**, *September*, 17.
(4) Parmon, V. N.; Panov, G. I.; Uriarte, A.; Noskov, A. S. *Catal. Today* **2005**, *100*, 115.
(5) Nowińska, K.; Wącław, A.; Izbińska, A. *Appl. Catal., A* **2003**, *243*, 225.
(6) Pérez-Ramírez, J.; Kondratenko, E. V. *Chem. Commun.* **2003**, 2152.
(7) Bulánek, R.; Wichterlová, B.; Novoveská, K.; Kreibich, V. *Appl. Catal., A* **2004**, *264*, 13.
(8) Kondratenko, E. V.; Pérez-Ramírez, J. *Appl. Catal., A* **2004**, *267*, 181.
(9) Pérez-Ramírez, J.; Gallardo-Llamas, A. *Appl. Catal., A* **2005**, *279*, 117.
(10) Buyevskaya, O. V.; Baerns, M. *Catalysis* **2002**, *16*, 155.
(11) Pérez-Ramírez, J.; Gallardo-Llamas, A. *J. Catal.* **2004**, *223*, 382.
(12) Pérez-Ramírez, J.; Gallardo-Llamas, A.; Daniel, C.; Mirodatos, C. *Chem. Eng. Sci.* **2004**, *59*, 5535.
(13) Gallardo-Llamas, A.; Mirodatos, C.; Pérez-Ramírez, J. *Ind. Eng. Chem. Res.* **2005**, *44*, 455.
(14) Pirutko, L. V.; Chernyavsky, V. S.; Uriarte, A. K.; Panov, G. I. *Appl. Catal., A* **2002**, *227*, 143.
(15) Meloni, D.; Monaci, R.; Solinas, V.; Berlier, G.; Bordita, S.; Rossetti, I.; Oliva, C.; Forni, L. *J. Catal.* **2003**, *214*, 169.
(16) Selli, E.; Rossetti, I.; Meloni, D.; Sini, F.; Forni, L. *Appl. Catal., A* **2004**, *262*, 131.
(17) Meloni, D.; Monaci, R.; Rombi, E.; Guimon, C.; Martinez, H.; Fechete, I.; Dumitriu, E. *Stud. Surf. Sci. Catal.* **2002**, *142A*, 167.
(18) Capek, L.; Kubánek, P.; Wichterlová, B.; Sobalík, Z. *Collect. Czech. Chem. Commun.* **2003**, *68*, 1805.
(19) Pérez-Ramírez, J. *J. Catal.* **2004**, *227*, 512.
(20) Pérez-Ramírez, J.; Kapteijn, F.; Groen, J. C.; Doménech, A.; Mul, G.; Moulijn, J. A. *J. Catal.* **2003**, *214*, 33.
(21) Lippens, B. C.; de Boer, J. H. *J. Catal.* **1965**, *4*, 319.
(22) Brunauer, S.; Emmet, P. H.; Teller, E. *J. Am. Chem. Soc.* **1938**, *60*, 309.
(23) van Konigsveld, H.; Jansen, J. C.; van Bekkum, H. *Zeolites* **1990**, *10*, 235.
(24) Sing, K. S. W.; Everett, D. H.; Haul, R. A. W.; Moscou, L.; Pierotti, R. A.; Rouquerol, J.; Siemieniewska, T. *Pure Appl. Chem.* **1985**, *57*, 603.
(25) Pérez-Ramírez, J.; Mul, G.; Kapteijn, F.; Moulijn, J. A.; Overweg, A. R.; Doménech, A.; Ribera, A.; Arends, I. W. C. E. *J. Catal.* **2002**, *207*, 113.
(26) Rouquerol, F.; Rouquerol, J.; Sing, K. S. W. In *Handbook of Porous Materials*; Schütz, F., Sing, K. S. W., Weitkamp, J., Eds.; Wiley-VCH: Weinheim, 2002; Vol. 1, p 250.
(27) Gorte, R. J. *Catal. Lett.* **1999**, *62*, 1.
(28) Busca, G. *Phys. Chem. Chem. Phys.* **1999**, *1*, 723.
(29) Parry, E. P. *J. Catal.* **1963**, *2*, 371.
(30) Buzzoni, R.; Bordiga, S.; Ricchiardi, G.; Lamberti, C.; Zecchina, A.; Bellussi, G. *Langmuir* **1996**, *12*, 930.
(31) Hughes, T. R.; White, H. M. *J. Phys. Chem.* **1967**, *71*, 2192.
(32) Jacobs, P. A.; Heylen, C. F. *J. Catal.* **1974**, *34*, 267.
(33) Selli, E.; Forni, L. *Microporous Mesoporous Mater.* **1999**, *31*, 129.
(34) Pérez-Ramírez, J.; Groen, J. C.; Brückner, A.; Kumar, M. S.; Bentrup, U.; Debbagh, N. M.; Villaescusa, L. A. *J. Catal.* **2005**, *232*, 318.
(35) Bordiga, S.; Buzzoni, R.; Geobaldo, F.; Lamberti, C.; Giamello, E.; Zecchina, A.; Leofanti, G.; Petrini, G.; Tozzolo, G.; Vlaic, G. *J. Catal.* **1996**, *158*, 486.
(36) Lehmann, G. *Z. Phys. Chem. Neue Folge* **1970**, *72*, 279.
(37) Patarin, J.; Tullier, M. H.; Durr, J.; Kessler, H. *Zeolites* **1992**, *12*, 70.
(38) Pérez-Ramírez, J.; Santosh Kumar, M.; Brückner, A. *J. Catal.* **2004**, *223*, 13.
(39) Ivanov, D. P.; Sobolev, V. I.; Panov, G. I. *Appl. Catal., A* **2003**, *241*, 113.
(40) Ivanov, D. P.; Rodkin, M. A.; Dubkov, K. A.; Kharitonov, A. S.; Panov, G. I. *Kinet. Catal.* **2000**, *41*, 850.
(41) Zhu, Q.; van Teeffelen, R. M.; van Santen, R. A.; Hensen, E. J. M. *J. Catal.* **2004**, *221*, 575.
(42) Hensen, E. J. M.; Zhu, Q.; van Santen, R. A. *J. Catal.* **2003**, *220*, 260.